Macromolecules

ARTICLE

pubs.acs.org/Macromolecules

Poly(ethylene oxide) Adsorption onto and Desorption from Silica Microspheres: New Insights from Optical Tweezers Electrophoresis

Jan A. van Heiningen* and Reghan J. Hill

Department of Chemical Engineering, McGill University, Montreal, Quebec H3A 2B2, Canada

ABSTRACT: By measuring the changing electrophoretic mobility of single optically trapped silica microspheres (radius $a \approx 0.4\,\mu$m) during poly(ethylene oxide) homopolymer adsorption and desorption, we study polymer-layer kinetics at various polymer solution flow rates, concentrations, molecular weights, and polydispersities. At polymer concentrations $c \lesssim 5$ ppm (mg L^{-1}), Péclet numbers $Pe \lesssim 20$, and Reynolds numbers $Re \ll 1$, the adsorbing layer growth is mass-transport-limited, with time scales ∼10 s that are resolved on the uniquely small, micrometer length scale of optical tweezers electrophoresis (OTE) experiments. However, during adsorption, layer growth becomes limited by surface diffusion, reconformation, and exchange processes. Two characteristic relaxation times are revealed by the OTE time series. The faster time scale increases with polymer concentration and plateaus to ∼3 s when $c \sim 10$ ppm. This reflects layer development kinetics limited by surface diffusion and reconformation. The slower time scale is ∼100 s and reflects polymer exchange, which thermodynamically favors large adsorbed coils when solutions are polydisperse. Desorption is even slower but occurs faster than expected by local-equilibrium theory, possibly because of high shear rates ∼100 s^{-1}. The dynamic states probed by OTE are often sufficiently far from equilibrium that they cannot be adequately described by theories for equilibrium polymer adsorption, mass-transport-limited kinetics, or kinetics based on local equilibrium.

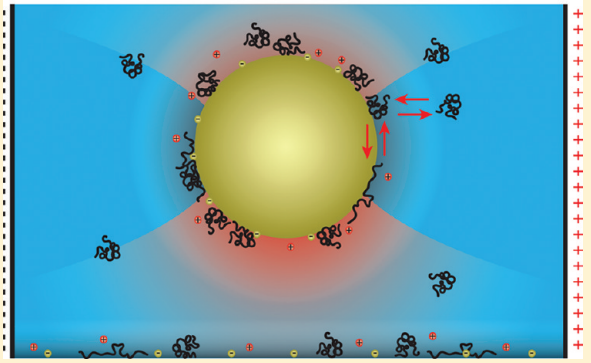

1. INTRODUCTION

Adsorbing polymers are added to colloidal dispersions to control stability and rheology.[18,23,41] Polymer adsorption is often a complex nonequilibrium process that involves transport of chains to the surface, attachment, relaxation and reconformation, and substitution while approaching equilibrium.[6] Adsorption can induce aggregation due to bridging or provide steric stability, depending on the attachment kinetics, shear rate, and concentrations of polymers and colloidal particles.

Many studies of polymer-adsorption kinetics have been conducted on macroscopic surfaces. The large length scales involved lead to mass-transport-limited kinetics that can be mixed with polymer reconformation and relaxation dynamics. Such methods include stagnation point flow, which monitors the quantity of adsorbed polymer due to an impinging jet.[12] Other methods involve capillary-tube streaming potentials, which furnish the temporal development of the spatially averaged hydrodynamic layer thickness during polymer adsorption.[13] Here, mass-transport-limited adsorption, which varies with distance from the tube inlet, follows the Lévêque equation. In these macroscopic geometries, the rapid injection of fluid required to obtain step changes in polymer concentration produces high shear rates, which can influence adsorption and desorption.[3,4]

For colloidal sized substrates rapidly immersed in dilute polymer solutions, the polymer diffusion time may be comparable to the polymer reconformation time, which itself may change during the course of layer development. The ability to form polymer bridges depends on the first several seconds of polymer adsorption. Polymers are more likely to bridge neighboring particles immediately following adsorption, while the time required for steric layers to develop is on the order of seconds.[1,36] Thus, it is unclear how adsorption dynamics gleaned from macroscale experiments might shed light on polymer adsorption onto colloidal sized substrates, and how such dynamics might influence bridging and flocculation.

Previous attempts to measure polymer adsorption onto colloidal particles were based on measuring an increase in hydrodynamic radius.[9,10] However, it is difficult to resolve such thin polymer layers on micrometer-sized particles. Moreover, adsorption kinetics are complicated by mixing hydrodynamics and fluid entrainment. To help avoid such complexities, we recently developed optical tweezers electrophoresis (OTE) to measure the electrophoretic mobility of a single microsphere during the adsorption of an uncharged homopolymer onto an initially bare surface.[43] Our instrument furnishes the electrophoretic mobility with a temporal resolution of about 0.5 s. While it does not directly measure hydrodynamic layer thickness, theoretical calculations reveal a close connection between the electrophoretic mobility and hydrodynamic layer thickness when the adsorbing polymer is uncharged and the particle charge is

Received: February 21, 2011
Revised: July 30, 2011
Published: September 28, 2011

dx.doi.org/10.1021/ma2003486 | *Macromolecules* 2011, 44, 8245–8260

Table 1. Poly(ethylene oxide) Molecular Weight Parameters

		manufacturer specifications			GPC			
PEO	manufacturer	M_p (kDa)	M_n (kDa)	M_w (kDa)	M_p (kDa)	M_n (kDa)	M_w (kDa)	M_z (kDa)
PEO120K	Acros Organics	100			101	42.2	119	276
PEO870K	Acros Organics	900			920	461	872	1338
PEO59K	Polymer Source		50	59				
PEO330K	Polymer Source		280	330	337	317	326	334
PEO480K	Polymer Source		430	482				

constant.[21,22] Moreover, the electrophoretic mobility is extremely sensitive to the polymer layer thickness, so the experiments are uniquely sensitive to polymer adsorption dynamics.

In this study, we monitored the electrophoretic mobility of a single silica microsphere during interaction with dilute poly(ethylene oxide) solutions. A brief description of the instrument and polymer solutions is provided in section 2. We describe approximate methods for calculating polymer adsorption and desorption rates and equilibrium layer thickness from electrophoretic mobility time series. In section 3, we present OTE adsorption and desorption results for various polymer solution concentrations, flow rates, and molecular weight distributions. In section 3.5, we show that thermodiffusion due to laser-induced heating may slightly decrease the polymer adsorption rate. Finally, we summarize our results in section 4.

2. THEORY AND METHODS

2.1. Optical Tweezers Electrophoresis. Concentrated ~1000 ppm poly(ethylene oxide) (PEO) solutions were prepared by dissolving polymers in DI water. The solutions were stored in UV-resistant bottles at 4 °C for a maximum of 3−4 weeks prior to final dilution in 1 mM NaCl for OTE experiments. The peak, number-averaged, weight-averaged, and z-averaged molecular weights, denoted M_p, M_n, M_w, and M_z, respectively, are summarized in Table 1. These were specified by the manufacturer and obtained from gel permeation chromatography (GPC) where applicable. The samples are denoted PEOxK, where x indicates M_w in kDa.

The experimental procedure for optical tweezer electrophoresis (OTE) adsorption experiments is described in detail elsewhere.[43] Briefly, polymer solutions and nonporous silica particle suspensions (radius $a \approx 400$ nm, monodisperse and nonfunctionalized, Bangs Laboratories, Inc.) were diluted in 1 mM NaCl. The final silica volume fraction was $\lesssim$0.1 ppm. OTE electrophoretic mobilities of a bare silica sphere were measured following abrupt exposure to flowing polymer solution. A microsphere was optically trapped at the center of a crossed parallel-plate channel at the gap position of zero steady electro-osmotic flow.[44] At this position, the local fluid velocity equals the gap-averaged fluid velocity. The solution and microsphere dispersions flow parallel to the electric field to reduce electro-osmotic flow artifacts during polymer adsorption. Note that the inlet tubes and syringes containing PEO solution were first equilibrated with adsorbing polymer by flowing excess polymer solution through the system. This ensured that the actual polymer solution concentration flowing past the optically trapped particle was stable and equal to the initially prepared solution concentration. Desorption experiments were performed by stopping the polymer flow while restarting the particle suspension flow. Thus, after a short 20 s transient, the polymer-coated particle could be reimmersed in flowing electrolyte without polymer. Electrophoretic mobilities were obtained using an oscillatory electric field at 50 Hz. At this frequency, the particle responds in a quasi-steady manner, and the background electro-osmotic flow is minimized.

The bare silica microspheres have electrophoretic mobilities μ_0^E that vary between about −3 and −4 μm cm V^{-1} s^{-1}, corresponding to ζ-potentials from about −45 to −60 mV. Thus, to isolate the influence of polymer adsorption on the OTE electrophoretic mobility time series $\mu^E(t)$, we adopt a reduced mobility

$$\mu(t) = 1 - \mu^E(t)/\mu_0^E \quad (1)$$

For adsorption experiments, a two time-scale empirical model

$$\mu(t) = \mu_{a,\infty}(1 - e^{-t/\tau_{a,1}}) + \mu_{a,1}(e^{-t/\tau_{a,1}} - e^{-t/\tau_{a,2}}) \quad (2)$$

was fit to reduced mobility time series, furnishing fitting parameters $\mu_{a,\infty}$, $\mu_{a,1}$, $\tau_{a,1}$, and $\tau_{a,2}$. Equation 2 guarantees that $\mu = 0$ when $t = 0$ and gives $\partial\mu/\partial t = \mu_{a,\infty}{\tau_{a,1}}^{-1} + \mu_{a,1}({\tau_{a,2}}^{-1} - {\tau_{a,1}}^{-1})$ when $t = 0$, and $\mu \rightarrow \mu_{a,\infty}$ as $t \rightarrow \infty$. Similarly, for desorption, a two time-scale model

$$\mu(t) = \mu_{d,\infty} + \mu_{d,1}(e^{-t/\tau_{d,1}} - e^{-t/\tau_{d,2}}) + (\mu_{d,0} - \mu_{d,\infty})e^{-t/\tau_{d,2}} \quad (3)$$

was fit to reduced mobility data, furnishing fitting parameters $\mu_{d,\infty}$, $\mu_{d,0}$, $\mu_{d,1}$, $\tau_{d,1}$, and $\tau_{d,2}$. Equation 3 yields $\mu = \mu_{d,0}$ when $t = 0$, and $\mu \rightarrow \mu_{d,\infty}$ as $t \rightarrow \infty$.

An example OTE adsorption/desorption experiment conducted with $c \approx 30$ ppm PEO120K on a single bare silica microsphere is shown in Figure 1. These data and all subsequent adsorption and desorption OTE reduced mobility time series are well described by eqs 2 and 3.

2.2. Electrophoretic Mobility and Polymer Adsorption Thermodynamics. Here we describe the theoretical framework for interpreting equilibrium polymer adsorption, hydrodynamics, and electrokinetics, which furnish the hydrodynamic layer thickness and adsorbed amount from long-time changes in OTE mobilities. These calculations extend the work of Cohen Stuart et al.[8] by combining equilibrium polymer segment density profiles with electrokinetic theory to predict particle electrophoretic mobilities. First, we numerically compute equilibrium polymer segment densities ψ for various polymer solution concentrations c and polymer molecular weights M_w, ultimately furnishing the adsorbed amount Γ. Then, the hydrodynamic layer thickness L_h and electrophoretic mobility μ^E are calculated from numerical solutions of the Debye−Brinkman equations for a flat plate.

Adsorbed flexible polymers form highly nonuniform layers comprising trains at the surface with decreasing concentrations

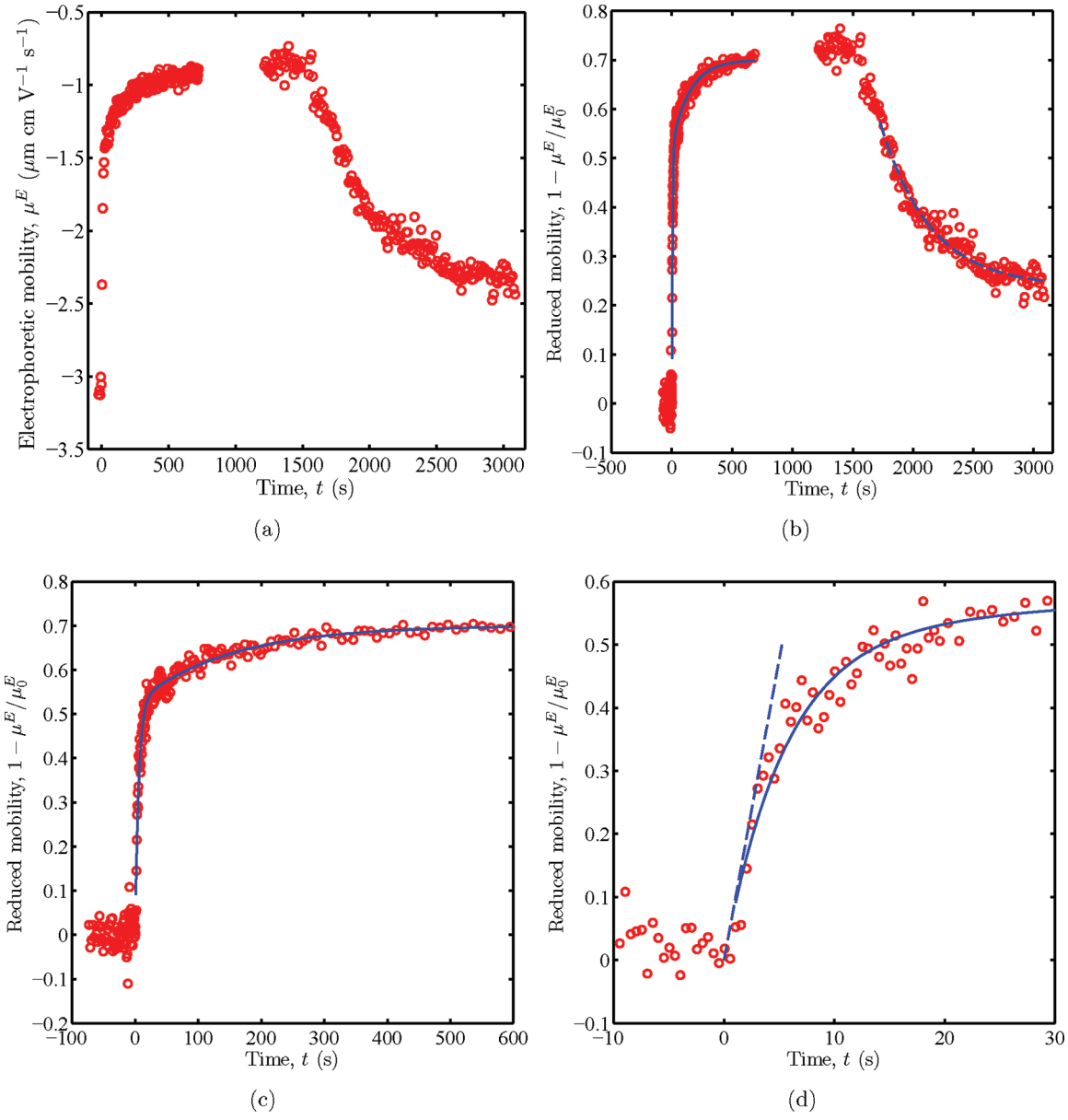

Figure 1. (a) Electrophoretic mobility μ^E time series for a bare silica microsphere (radius $a \approx 0.4$ μm) abruptly exposed to a $c \approx 30$ ppm PEO120K solution at time $t = 0$ s (adsorption). Desorption is initiated at $t \approx 1600$ s by abrupt re-exposure to flowing electrolyte without polymer. (b)−(d) Reduced electrophoretic mobility $\mu = 1 - \mu^E/\mu_0^E$ time series with details of adsorption at long (c) and short (d) times. Curved lines are least-squares fits of eq 2 for 0 s $\lesssim t \lesssim$ 600 s (solid) and eq 3 for $t \gtrsim 1600$ s (dashed). The straight dashed line in (d) is tangent to the adsorption curve at $t = 0$ s.

of loops and tails toward the bulk solution. We calculate segment densities for PEO adsorbed from water onto silica using a continuum approximation[16] of the well-known Scheutjens−Fleer lattice adsorption theory.[38,39] Here, statistical polymer segments occupy sites on a lattice with spacing l_s between nearest neighbors. We present results for a cubic lattice with the adsorbing surface located at $z = 0$. Therefore, the center of the train layer is located at $z_1 = l_s/2$, with the loop and tail layers at $z_n = (n - 1/2)l_s$ with $n = 2, 3, 4, ...$ For PEO/water/silica, we adopted a Flory−Huggins parameter $\chi = 0.4$,[33,42] and a net surface-segment exchange enthalpy $\chi_s = k_B T$.[40] The statistical segment length $l_s = 0.516$ nm and the Kuhn segment molar mass $m_s = 71$ g mol^{-1}. Equating the volume of a cube with length l_s to the volume of a statistical number of monomer segments with length $l_m = 0.44$ nm,[35] i.e., $l_s^3 \approx l_m^3 m_s/m_m$, furnishes l_s. Here, the PEO monomer (C_2OH_4) segment molar mass $m_m = 44$ g mol^{-1}. Note that l_s is approximately equal to the statistical segment size in a polymer melt with density $\rho_p \approx 1.2$ g cm^{-3}, i.e., $[m_s/(N_A \rho_p)]^{1/3} \approx 0.46$ nm.

The segment density ψ_n is the probability of a site at lattice index $n = 1, 2, 3, ...$ being occupied by a train, loop, or tail segment. Calculated equilibrium segment densities are shown in Figure 2a−c as a function of polymer solution concentration and chain length. As predicted by the Scheutjens−Fleer theory, the loop contribution dominates close to the surface. At large distances from the surface, the tail contribution, which falls off less rapidly than the loop contribution, dominates. The profile densities are weakly dependent on polymer concentration, with a measurable adsorbed amount at concentrations as low as $c \sim 10^{-100}$ ppm for PEO120K.

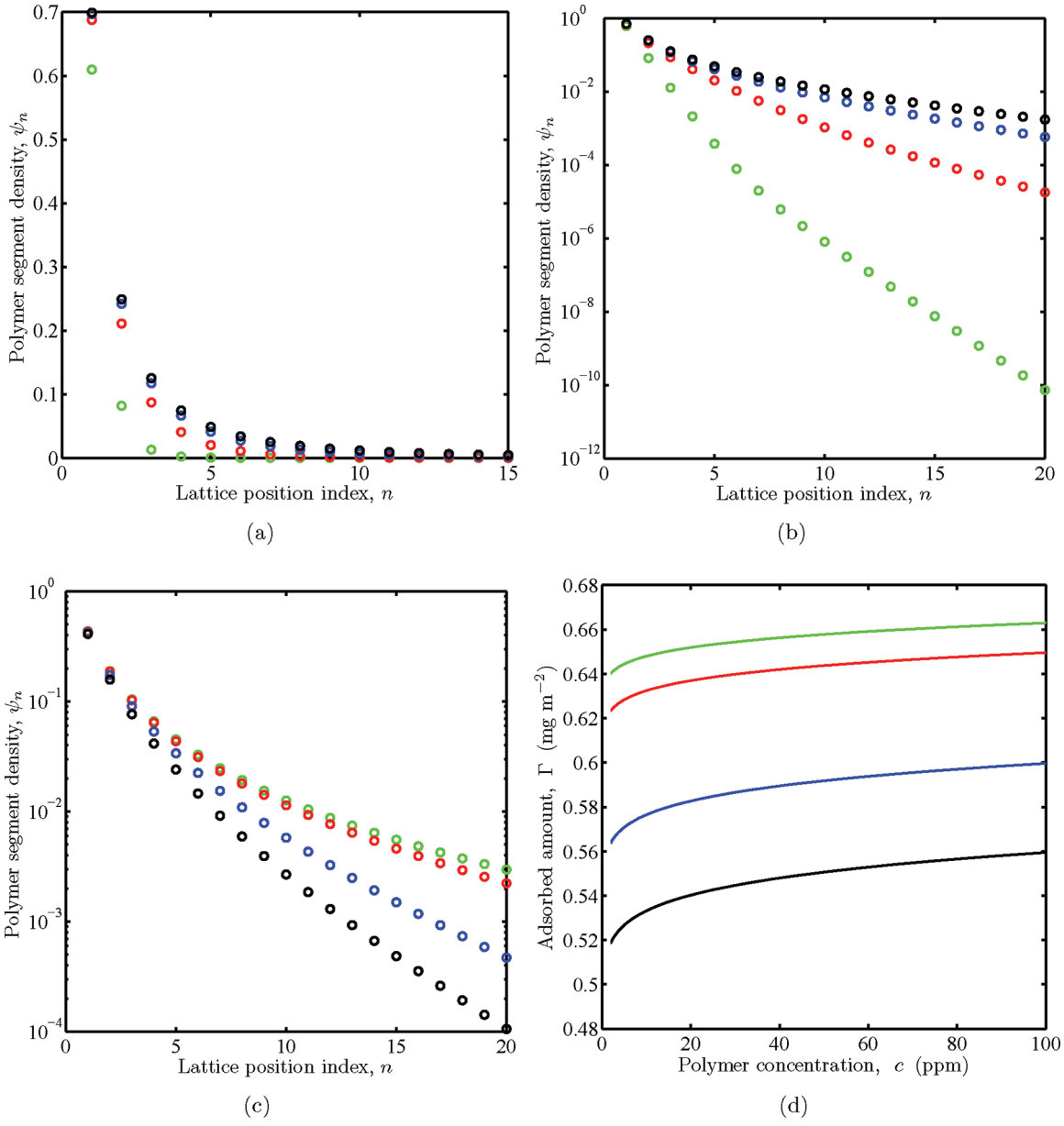

Figure 2. Continuum approximation of the Scheutjens−Fleer lattice theory for poly(ethylene oxide) (PEO) adsorption from water onto silica. Statistical segment length l_s = 0.516 nm with molecular weight m_s = 71 g mol^{-1} (cubic lattice), surface-segment exchange enthalpy $\chi_s = k_BT$, and Flory−Huggins parameter χ = 0.4. Top: polymer solution concentration c = 100 (black), 1 (blue), 10^{-10} (red), and 10^{-100} ppm (green). Bottom: molecular weight M_w = 59 (black), 120 (blue), 480 (red), and 870 kDa (green). (a) Linear and (b) logarithmic segment density ψ_n vs lattice position index n = 1, 2, 3, ... [$z_n = (n - 1/2)l_s$] with chain length $N = M_w/m_s \approx 1690$ (M_w = 120 kDa). (c) ψ_n vs n with c = 1 ppm, and (d) adsorbed amount Γ vs c.

The adsorbed amount (per unit area)

$$\Gamma = \frac{m_s}{l_s^2 N_A} \sum_{n=1}^{\infty} \psi_n \tag{4}$$

sums the contributions from train, tail, and loop segments. The equilibrium adsorption isotherm calculations in Figure 2d are very similar to experimentally measured isotherms for PEO/water/silica.[12,30,46] Note that the adsorbed amount is much more sensitive to polymer molecular weight than polymer concentration.

As uncharged polymer adsorbs onto a bare, charged microsphere, it very slightly increases the particle size, but the thin layer significantly reduces the electrophoretic mobility by its influence on the electrophoretic retardation force. We calculate the hydrodynamic layer thickness $L_h \ll a$ from the one-dimensional (flat-plate approximation) Debye−Brinkman equation

$$\frac{\partial^2 u}{\partial z^2} = \frac{u}{l_B^2} \tag{5}$$

where u is the fluid velocity. Note that the square of the Brinkman screening length $l_B^2 = l_s^3/(6\pi a_s \psi)$ characterizes the hydrodynamic permeability. The boundary conditions are $u = 0$ at $z = 0$ (no-slip), and $u \rightarrow \dot{\gamma}\,(z - L_h)$ as $z \rightarrow \infty$, where $\dot{\gamma}$ is the far-field shear rate.

dx.doi.org/10.1021/ma2003486 |*Macromolecules* 2011, 44, 8245–8260

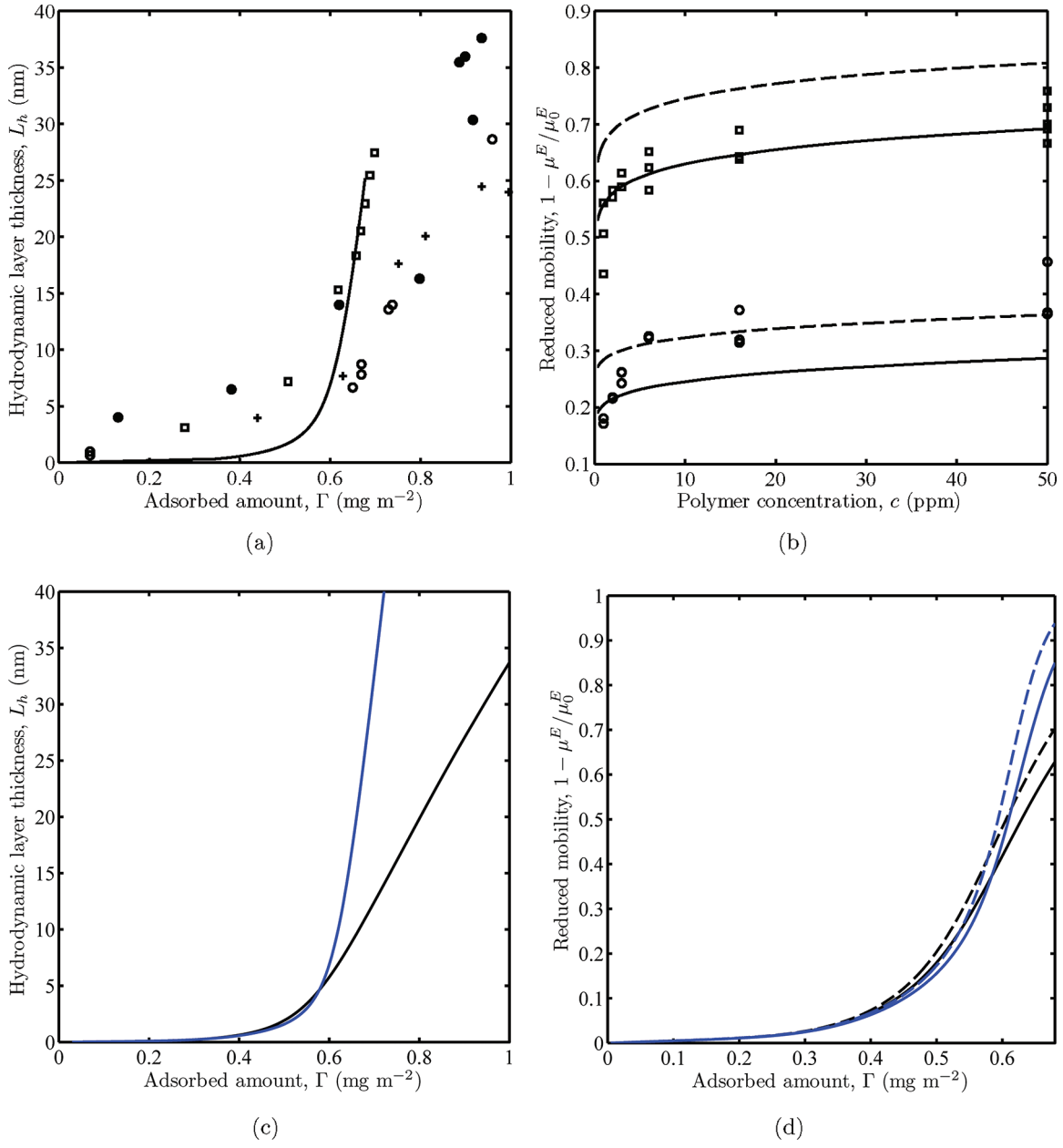

Figure 3. Equilibrium hydrodynamic layer thickness L_h, electrophoretic mobility μ^E, and adsorbed amount Γ from flat-plate models based on calculated equilibrium polymer segment density profiles: $\zeta = -2k_BT/e$ with 1 mM NaCl electrolyte. Solid lines are L_h and μ^E from eqs 5 and 7, respectively, with $a_s \approx 0.039$ nm. Dashed lines are μ^E from eq 6 with L_h from eq 5. (a) L_h vs Γ for PEO480K (theory) with experimental data from Lafuma et al.[31] for M_w = 1100 (open circles), 2000 (filled circles), and 570 kDa (pluses) and from Wind and Killmann[46] for M_w = 900 kDa (squares). (b) Reduced electrophoretic mobility $1-\mu^E/\mu_0^E$ vs polymer concentration c for PEO59K (circles) and PEO480K (squares) from OTE with corresponding theory (lines). (c) L_h vs Γ and (d) $1-\mu^E/\mu_0^E$ vs Γ for PEO59K (black lines) and PEO480K (blue lines).

The electrophoretic mobility μ^E can be transformed to a hydrodynamic layer thickness using

$$\tanh\left(\frac{e\eta\mu^E}{4\varepsilon\varepsilon_0 k_B T}\right) = \tanh\left(\frac{e\eta\mu_0^E}{4\varepsilon\varepsilon_0 k_B T}\right) e^{-\kappa L_h} \quad (6)$$

where μ_0^E is the bare particle mobility and κ^{-1} is the Debye length. Note that eq 6 is for uniform layers with $\kappa a \gg 1$ and $l_B \lesssim L_h$.[34] It is often used to ascertain the thickness of uncharged, uniform polymer layers from electrophoresis and streaming potential measurements.[7,17]

We calculate the electrophoretic mobility for arbitrary layer profiles when $\kappa a \gg 1$ by adding an electrical body force to eq 5, yielding

$$\frac{\partial^2 u}{\partial z^2} = \frac{u}{{l_B}^2} + \frac{\varepsilon\varepsilon_0 E}{\eta}\frac{\partial^2 \psi_e}{\partial z^2} \quad (7)$$

where E is the electric field magnitude, ψ_e is the equilibrium electrostatic potential, and $\varepsilon\varepsilon_0$ is the electrolyte dielectric permittivity. The boundary conditions are $u = 0$ at $z = 0$ (no-slip), and $\partial u/\partial z \rightarrow 0$ as $z \rightarrow \infty$. In a symmetric electrolyte, ψ_e is

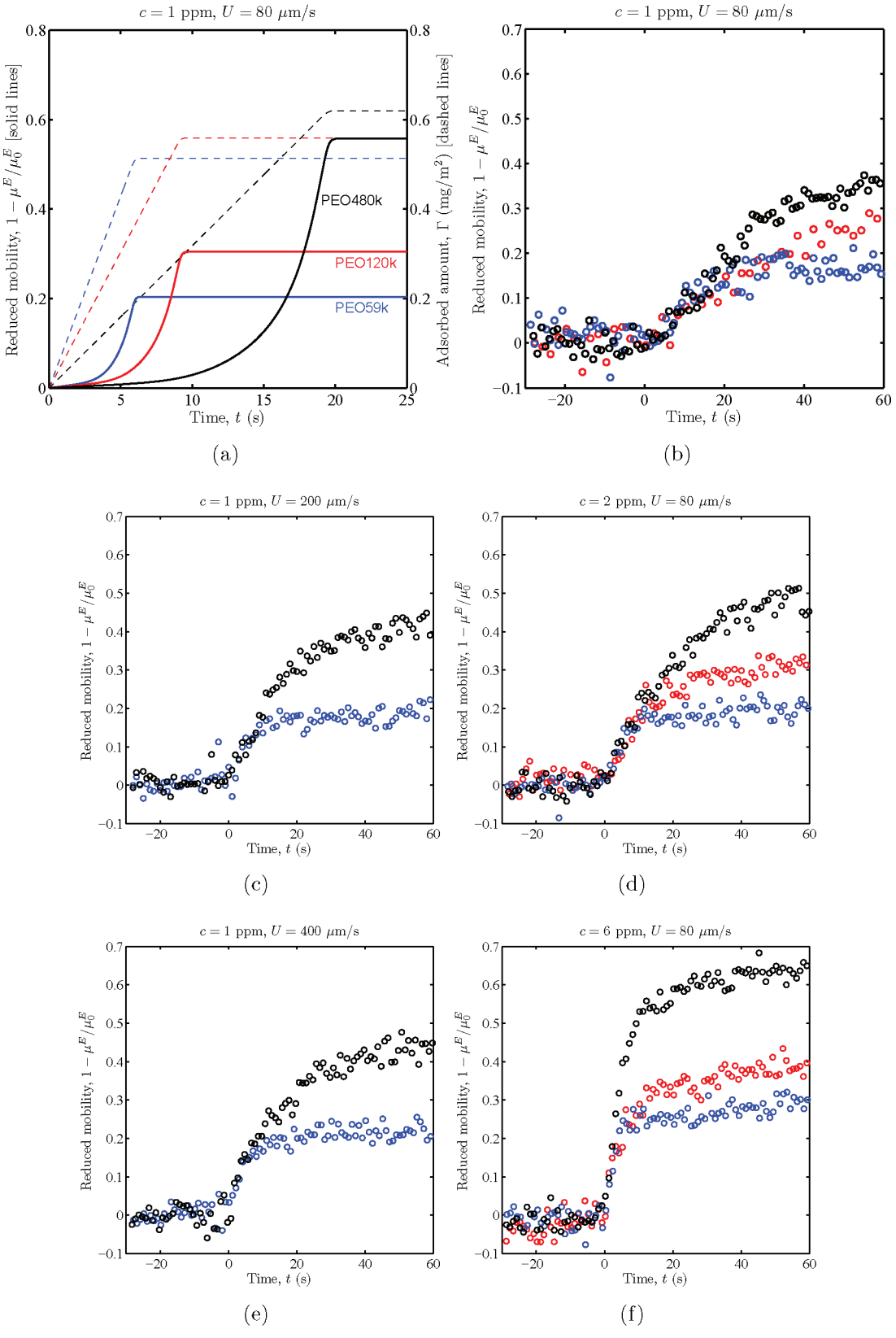

Figure 4. Reduced electrophoretic mobility $1 - \mu^E/\mu_0^E$ time series for bare silica microspheres (radius $a \approx 0.4\,\mu$m) abruptly exposed to PEO solutions at $t \approx 0$ s: PEO59K (blue), PEO120K (red), and PEO480K (black). (a) Theory (adsorbed amount and mobility) based on local equilibrium according to eq 18 with c = 1 ppm and U = 80 μm s^{-1}. (b)−(f) OTE data with c and U identified in each panel.

dx.doi.org/10.1021/ma2003486 |*Macromolecules* 2011, 44, 8245–8260

obtained from the Poisson−Boltzmann equation, giving[23]

$$\tanh\left(\frac{ze\psi_e}{4k_BT}\right) = \tanh\left(\frac{ze\zeta}{4k_BT}\right)e^{-\kappa z} \quad (8)$$

where ze, k_BT, and ζ are respectively the ion charge, thermal energy, and electrostatic surface potential.

Substituting

$$\frac{\partial^2\psi_e}{\partial z^2} = \frac{4k_BT\kappa^2}{ze}\frac{y(1+y^2)}{(1-y^2)^2} \quad (9)$$

with

$$y = \tanh\left(\frac{ze\zeta}{4k_BT}\right)e^{-\kappa z} \quad (10)$$

from eq 8 into eq 7 furnishes an ordinary differential equation for u from which the particle electrophoretic mobility $\mu^E = -u/E$ as $z \to \infty$ is obtained.[a]

As shown in Figure 3a,b, reasonable correspondence of the foregoing flat-plate models is achieved with our OTE and literature mobility and hydrodynamic layer thickness data when $a_s \approx 0.039$ nm. Moreover, the order of magnitude of $l_s^3/(6\pi a_s) \approx 1$ nm^2 is consistent with sedimentation experiments for polymer solutions.[32] Comparing the dashed and solid lines in Figure 3b,d reveals that eq 6 furnishes particle electrophoretic mobilities that are ~10% larger than obtained from eq 7.

2.3. Adsorption and Desorption Kinetics. Here we attempt to quantify adsorption and desorption kinetics based on simple mass-transport mechanisms, making an assumption of local equilibrium. While this model is tremendously oversimplified, it is the only means presently at our disposal to interpret the OTE kinetics. Despite its obvious shortcomings, comparing such predictions with OTE data is a valuable exercise for quantifying the merits and limitations of the theory and its underlying assumptions.

For bare microspheres with radius $a \approx 0.4$ μm abruptly exposed to a solution of adsorbates with diffusion coefficient $D \approx 2 \times 10^{-11}$ m^2 s^{-1} (PEO, $M_w = 100$ kDa), the diffusion time scale $a^2/D \approx 8$ ms. Thus, the small characteristic length scale in these experiments ensures that even the largest polymer chains can rapidly establish a quasi-steady diffusion flux.

The time rate of change of surface coverage θ can be written

$$\frac{\partial\theta}{\partial t} = k_a c_s - k_d\theta = k_m(c - c_s) \quad (11)$$

where k_a, k_d, and k_m are the surface attachment, detachment, and mass-transport rate constants, respectively, c is the bulk polymer concentration, and c_s is the polymer solution concentration at the particle surface $r = a$. Eliminating c_s from eq 11 gives

$$\frac{\partial\theta}{\partial t} = \frac{k_a k_m}{k_a + k_m}c - \frac{k_d k_m}{k_a + k_m}\theta \quad (12)$$

so the initial kinetics for an initially bare surface are described by

$$\frac{\partial\theta}{\partial t}(t = 0) = k_e c \quad (13)$$

where

$$k_e = \frac{k_a k_m}{k_a + k_m} \quad (14)$$

defines an effective rate constant.

For viscous flow past a sphere with Reynolds number $Re = Ua/\nu \ll 1$[5]

$$k_m = \frac{DSh}{a\Gamma_0} \quad (15)$$

where the Sherwood number

$$2Sh \approx 1 + (1 + 2Pe)^{1/3} \quad (16)$$

and the Péclet number $Pe = Ua/D$. Here, U is the undisturbed fluid velocity at the optical trap, ν is the kinematic viscosity, and the PEO diffusion coefficient[11,12]

$$D\ (\text{m}^2\ \text{s}^{-1}) \approx 1.46 \times 10^{-8}[M_w\ (\text{Da})]^{-0.571} \quad (17)$$

In eq 15, we have set $\theta = \Gamma/\Gamma_0$, where Γ_0 is the equilibrium mass coverage. Note that reflectometry experiments indicate that $\Gamma_0 \approx 0.7$ mg m^{-2} when $M_w \approx 50-1000$ kDa and $c \approx 10-100$ ppm. As a useful point of reference, we note that the mass coverage corresponding to the mass of a 100 kDa PEO chain occupying an area equal to the square of its hydrodynamic radius $R \equiv k_BT/(6\pi\eta D)$ is $M_w/(N_AR^2) \approx 0.8$ mg m^{-2}, which is considerably higher than the value $\Gamma \approx 0.6$ mg m^{-2} achieved when PEO adsorbs onto silica from aqueous solution.

Local equilibrium implies that c_s and Γ are related by the equilibrium adsorption isotherm,[13] which occurs when the adsorption and desorption rate constants are large compared to the mass transfer rate constant. Indeed, from eq 11, $c_s = [c + (k_d/k_m)\theta]/(k_a/k_m + 1) \to (k_d/k_a)\theta$ when $k_m \ll k_a$ and $k_m \ll k_d$. Note also that polymer reconformation kinetics must be sufficiently fast for k_a and k_d to be be considered constant. With these assumptions, eqs 11 and 15 give

$$\frac{\partial\Gamma}{\partial t} = \frac{DSh}{a}[c - c_s(\Gamma)] \quad (18)$$

with initial condition $\Gamma(t = 0) = 0$ (adsorption) or $\Gamma(t = 0) = \Gamma(c_0)$ (desorption) with c_0 the bulk polymer concentration prior to desorption. Thus, eq 18 and the theory in section 2.2 furnish $\Gamma(t)$ and $\mu_E(t)$.

Several local-equilibrium adsorption time series are shown in Figure 4a, with the mobility calculated numerically according to eq 7. The mobilities (solid lines) exhibit a strikingly different behavior than the adsorbed amounts (dashed lines), and both are qualitatively different than the OTE mobility time series seen in panels b−f. According to local equilibrium, the adsorbed amount increases linearly up to full coverage, with a rate that decreases with the polymer molecular weight, reaching equilibrium at a time that increases with molecular weight. The accompanying reduced mobility time series increase with an increasing rate, rapidly saturating as the adsorbed amount reaches equilibrium. However, OTE mobility time series approach equilibrium more slowly and with a monotonically decreasing rate. These differences suggest that slow, nonequilibrium processes are at play. For example, increasingly hindered adsorption would slow the overall dynamics, while hindered chain reconformation would produce thicker (less compact) layers at shorter times. Together, hindered adsorption and chain reconformation seem to explain the more immediate increase in reduced mobility and overall slower approach to equilibrium.

Note that Monte Carlo simulations indicate that polymer rearrangements for single coils physically adsorbing to a bare surface occur on subsecond time scales.[26] Thus, the assumption of local equilibrium is likely to be reasonable only during the first

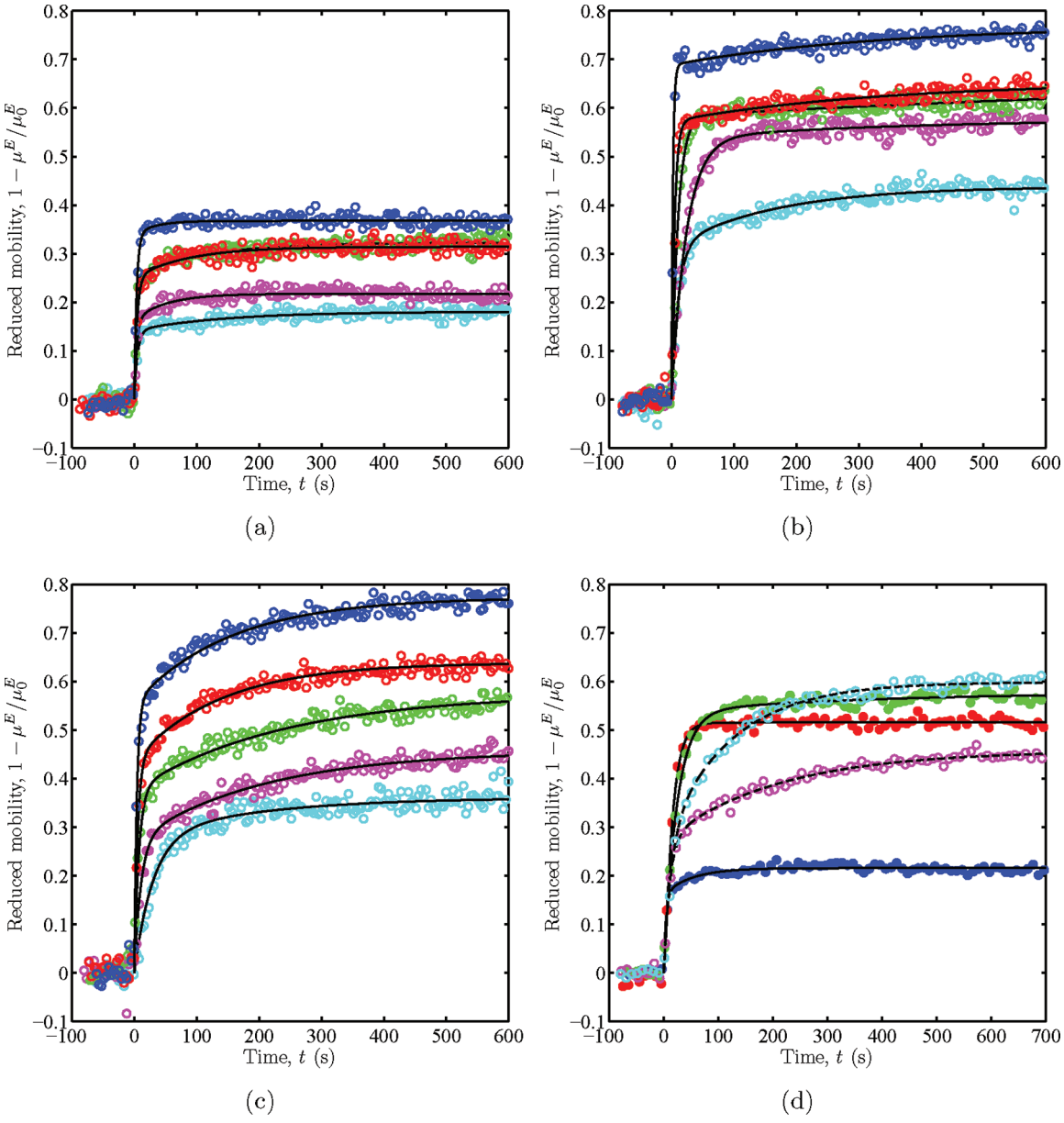

Figure 5. Reduced electrophoretic mobility $\mu = 1 - \mu^E/\mu_0^E$ time series for bare silica microspheres (radius $a \approx 0.4$ μm) abruptly exposed to PEO solutions at $t = 0$ s: $c \approx 50$ (blue), 16 (red), 6 (green), 2 (magenta), and 1 ppm (cyan) for (a) monodisperse PEO59K, (b) monodisperse PEO480K, and (c) polydisperse PEO120K. Lines are least-squares fits of eq 2 for $t \gtrsim 0$ s. (d) $c \approx 2$ ppm monodisperse (filled symbols with solid lines) and polydisperse (open symbols with dashed lines) PEO solutions for PEO59K (blue), PEO330K (red), PEO480K (green), PEO120K (magenta), and PEO870K (cyan).

second, at which time the adsorbed amount is very small and the kinetics become mass-transfer-limited.

The approach to full coverage, which is well resolved by the OTE experiments, reflects nonequilibrium layer dynamics. Figure 4a indicates that much of the polymer mass is adsorbed by the time the mobility begins to change significantly. Comparing to the OTE data in Figure 4b, for example, suggests that nonequilibrium processes likely occur when most of the polymer is already attached. Note that the experimentally observed approach to equilibrium is significantly slower than expected from the local-equilibrium theory.

3. RESULTS

3.1. OTE Equilibrium Adsorption. Several representative mobility time series for bare silica microspheres abruptly exposed to PEO solutions with various molecular weights and concentrations are shown in Figure 5. The equilibrium hydrodynamic layer thickness and reduced electrophoretic mobility are more sensitive to polymer concentration c and molecular weight M_w than the adsorbed amount Γ. Comparing Figures 5a,b with 5c suggests that polydispersity slows the dynamics: the layer thickness increases over several minutes as larger coils displace smaller adsorbed chains. With $c \approx 2$ ppm, Figure 5d shows how the adsorbed layer thickness increases with polymer molecular weight and, again, how polydispersity (open symbols) slows the dynamics.

The mobility time series in Figure 5 are well described by eq 2 (lines). For monodisperse polymer solutions, however, a single time constant is often sufficient. Thus, fitting eq 2 can infer unacceptable layer thicknesses as $t \rightarrow \infty$. Therefore, we

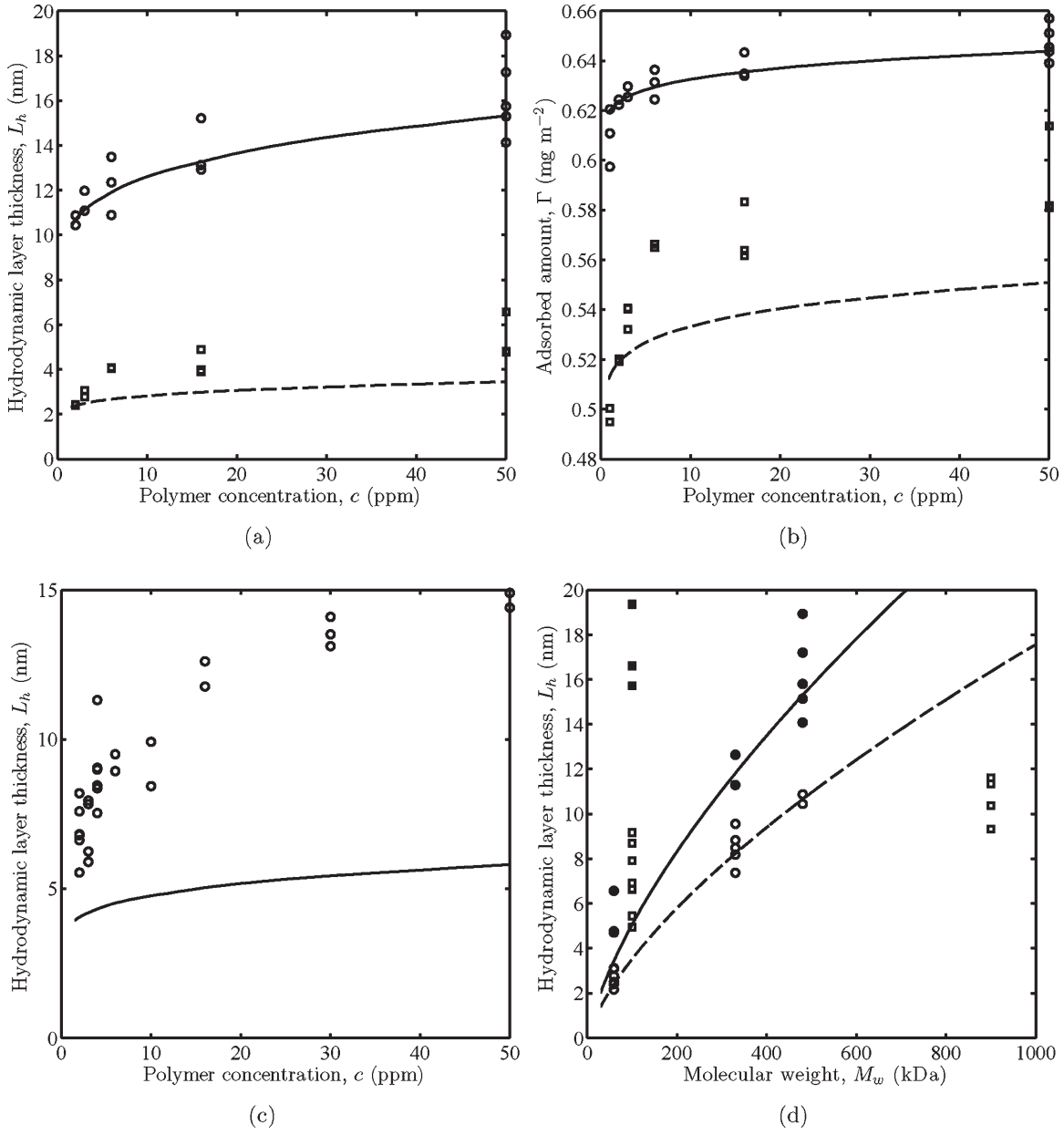

Figure 6. Hydrodynamic layer thickness L_h and adsorbed amount Γ of PEO adsorbed on initially bare silica microspheres (radius $a \approx 0.4\ \mu$m) ≈ 700 s following abrupt exposure to polymer solutions. Solid and dashed lines are theoretical predictions from eqs 5 and 7 for equilibrium. (a) L_h and (b) Γ vs concentration c for PEO480K (circles and solid lines) and PEO59K (squares and dashed lines). (c) L_h vs c for PEO120K. (d) L_h vs M_w with $c \approx 50$ ppm (OTE, filled symbols; theory, solid lines) and $c \approx 2$ ppm (OTE, open symbols; theory, dashed lines) for monodisperse (circles) and polydisperse (squares) PEO solutions.

approximate the equilibrium mobility as the value furnished by eq 2 at $t \approx 700$ s, which we assume is sufficient for the layers to adopt an equilibrium profile that corresponds to the adsorbed amount at that time.[29,30] Note that the silanol groups on silica are known to catalyze PEO decomposition, with a time scale of hours. While this will reduce the polymer layer thickness and excess solution molecular weight,[29] the trapped microspheres in OTE experiments are exposed to an infinite excess of fresh PEO, thereby avoiding continuous layer decomposition.

Equilibrium layers ≈700 s after abrupt exposure to polymer solutions are compared in Figure 6. Using the OTE reduced mobility data, the adsorbed amounts Γ in panel b are calculated from equilibrium curves $\Gamma(\mu,M_w)$, e.g., Figure 3d (solid lines). Figure 6a,b shows that Γ is less sensitive to c and M_w than L_h. Panels c and d reveal that L_h is significantly larger than expected for polydisperse polymers (PEO120K) based on M_w. However, the final reduced mobility for the highest molecular weight polymer PEO870K is smaller than expected by the Scheutjens−Fleer theory.[8] Since this sample was about one year older (stored in a dry state before experiments), it may have undergone oxidative/thermal degradation,[20] which is expected to have a more significant impact on high molecular weight polymers. For polymer concentrations $c \approx 50$ ppm, the OTE results in panel d for monodisperse polymers (PEO59K, PEO280K, PEO480K) are consistent with literature[30,31] where the hydrodynamic layer thickness L_h scales as $M_w^{0.5}$. No literature data exist for polymer

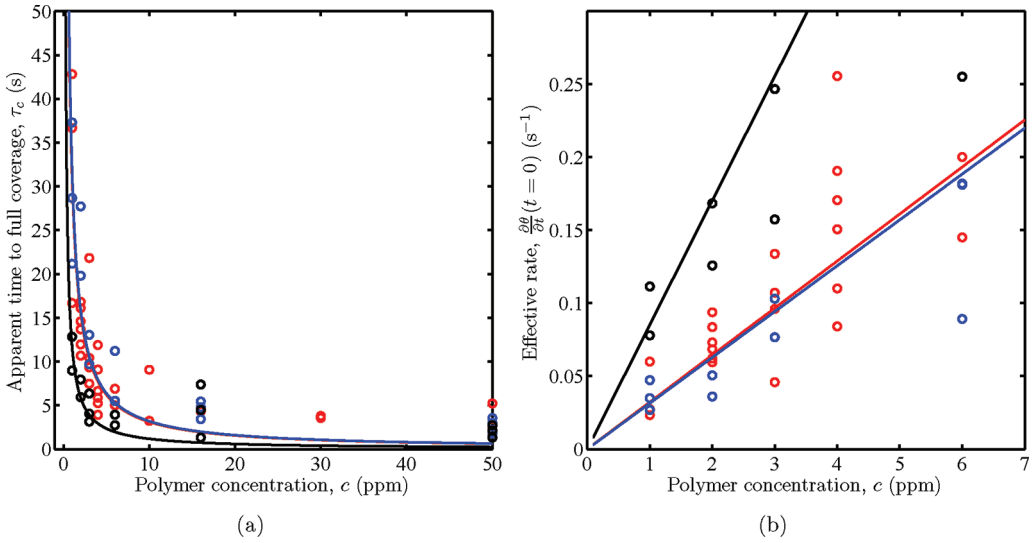

Figure 7. (a) Apparent time to full coverage $\tau_c \approx [(\partial\theta/\partial t)(t=0)]^{-1}$ vs polymer concentration c: PEO59K (black), PEO480K (blue), and PEO120K (red). Lines are fits of eq 13 to the OTE data with $c \lesssim 5$ ppm. (b) τ_c replotted as an effective short-time adsorption rate $\tau_c^{-1} \approx (\partial\theta/\partial t)(t=0)$ vs c.

concentrations as low as 2 ppm, where OTE data yields $L_h \propto M_w^{0.65}$, in agreement with the Scheutjens—Fleer theory. For many other absorbents, such as latex particles[27] or cellulose acetate,[28] PEO layers are thicker and take much longer to reach equilibrium.

3.2. OTE Adsorption Kinetics. *3.2.1. Effect of Polymer Concentration.* Polymer adsorption kinetics are difficult to quantify because of the nonequilibrium dynamics. Nevertheless, to expedite a quantitative interpretation of the OTE adsorption dynamics, we define an apparent time to full coverage

$$\tau_c \equiv \frac{\mu^\infty}{\frac{\partial\mu}{\partial t}(t=0)} \approx \left[\frac{\partial\theta}{\partial t}(t=0)\right]^{-1} \quad (19)$$

where the reduced mobility at equilibrium $\mu^\infty \approx \mu(c = 10\ \text{ppm})$; recall that Figure 3b shows that μ is nearly constant when $c \gtrsim 10$ ppm. Thus, for PEO59K, PEO120K, PEO480K, and PEO870K solutions, $\mu^\infty \approx 0.25$, 0.36, 0.63, and 0.70, respectively.

The apparent time to full coverage τ_c from eq 19 is shown in Figure 7. The initial PEO adsorption rate onto a bare microsphere increases with c when $c \lesssim 10$ ppm. From eq 13, we obtain an effective rate constant k_e from the slopes of the fitted lines with $c \lesssim 5$ ppm (e.g., Figure 1). Thus, for PEO59K, PEO120K, and PEO480K, we find $k_e \approx 0.086$, 0.032, and 0.031 $\text{ppm}^{-1}\ \text{s}^{-1}$, respectively, as shown in Figure 7b. These rates have the same dependence on polymer concentration as the theoretical mass-transport rate constant from eq 15, which furnishes, respectively, $k_m \approx 0.123$, 0.087, and 0.045 $\text{ppm}^{-1}\ \text{s}^{-1}$. Nonequilibrium polymer reconformation and attachment kinetics and the approximation in eq 19 may account for differences between the foregoing effective rate constants k_e and the theoretical mass-transport rate constants k_m.

3.2.2. Effect of Viscous Flow Rate Past a Sphere. The PEO adsorption rate onto silica microspheres increases with flow rate, as shown in the left panels of Figure 8. Here, OTE apparent times to full coverage τ_c are calculated from eq 19, which are compared to mass-transport limited adsorption ($k_a = \infty$) from eqs 13−17. The corresponding equilibrium hydrodynamic layer thicknesses at ≈700 s are nearly independent of flow rate (or Péclet number), as shown in the right panels. In the bottom panels, the polydisperse PEO layers develop much more slowly than expected from theory based on mass transport alone.

3.3. OTE Desorption Kinetics. PEO clearly desorbs from a trapped polymer-coated microsphere immersed in a continuous flow of pure electrolyte. Nearly all polymer desorbs after ∼1 h. As shown in Figure 9a, the adsorption is mostly reversible upon subsequent re-exposure to polymer solution.

Equations 2 and 3 respectively were fit to the adsorption and desorption reduced mobility time series. For desorption, there is a short transient ∼30 s for PEO solution to be displaced at the microsphere location by flowing electrolyte. Several reduced mobility time series for PEO59K, PEO120K, PEO330K, PEO480K, and PEO870K are plotted in Figure 9b with polymer concentration $c \approx 2$ ppm and best-fit lines from eqs 2 and 3.

OTE desorption kinetics are more rapid for the lower molecular weight polymers, which indicate nearly complete desorption ≈1500 s after shutting off polymer solution flow, as seen in Figure 9c. Local equilibrium theory suggests that desorption occurs more slowly, especially for elapsed times ≳1000 s. The higher desorption rates observed in experiments may be due to several factors, including (i) high fluid shear rates $\dot{\gamma} \sim U/a \sim 100\ \text{s}^{-1}$ at the trapped particle surface, (ii) slow dissolution of the silica particle itself,[24] and (iii) catalytic decomposition of the adsorbed PEO by surface silanol groups. Note that the calculations in Figure 9d are for monodisperse polymer with M_w = 120 kDa, whereas experiments were performed with polydisperse PEO120K, which may explain quantitative discrepancies. Here, for elapsed times ∼1500 s, the experiments indicate that the remaining layer thickness increases with c. For polydisperse polymer solutions, the proportion of higher molecular weight polymers adsorbed at equilibrium may increase with c, and (as seen in Figure 9c) these take longer times to desorb.

3.4. Qualitative Effects of Polydispersity. In dilute polydisperse polymer solutions, the higher molecular weight species are preferentially adsorbed at equilibrium because the entropy of mixing is greater for small chains.[14,18] For bidisperse PEO adsorbing onto macroscale silica surfaces, the final approach to equilibrium takes longer than local equilibrium predictions when

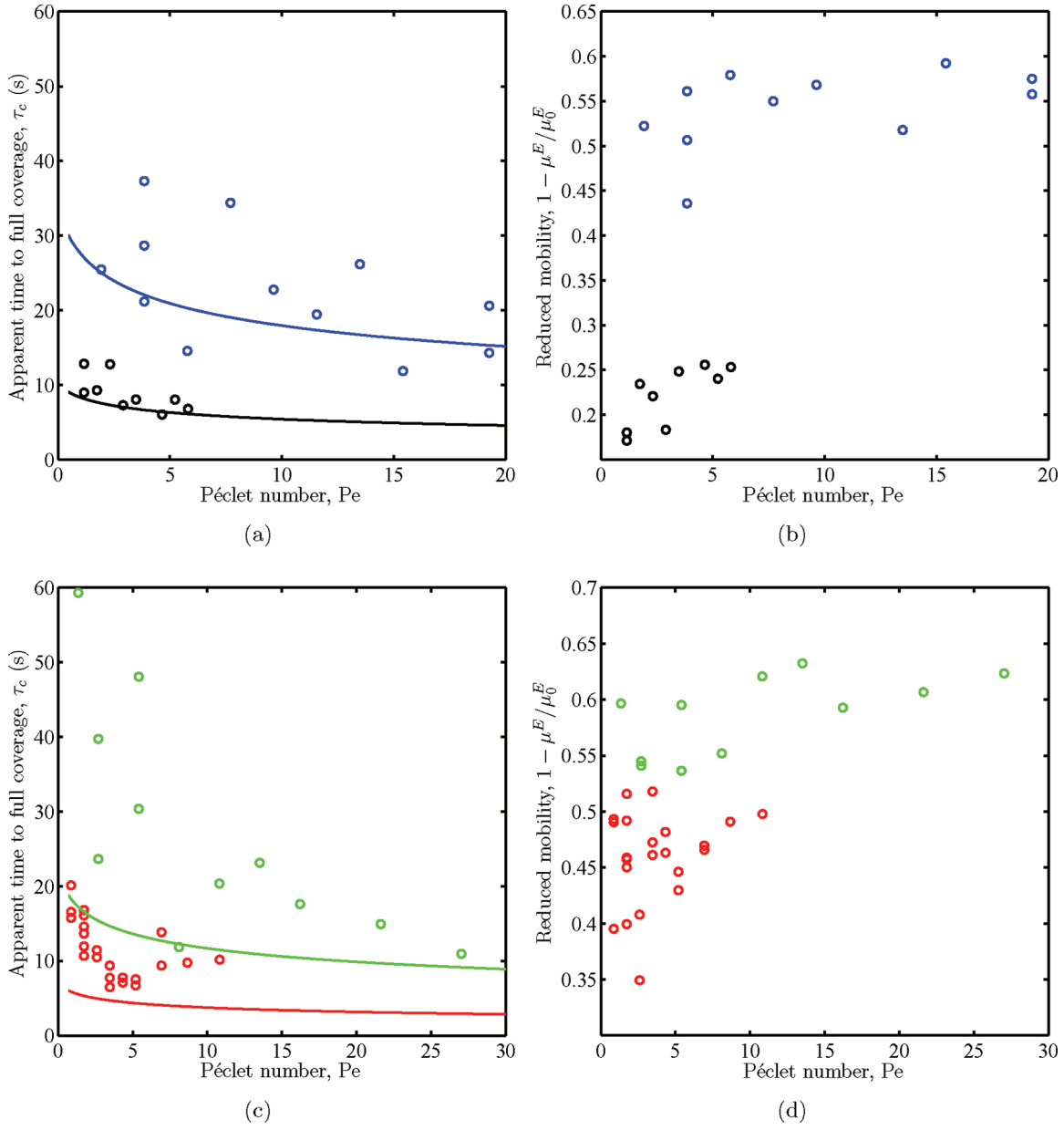

Figure 8. Apparent time to full coverage $\tau_c \approx [(\partial\theta/\partial t)(t=0)]^{-1}$ from eq 19 (left) and corresponding equilibrium reduced mobilities (right panels) vs Péclet number *Pe*. Top: monodisperse $c \approx 1$ ppm PEO59K (black) and PEO480K (blue). Bottom: polydisperse $c \approx 2$ ppm PEO120K (red) and PEO870K (green). Lines are τ_c from eqs 13−17 for mass-transport-limited adsorption.

the smaller adsorbed PEO species has $M_w \gtrsim 120$ kDa. Here, replacement of smaller adsorbed coils with larger ones is hindered by a significant energy barrier.[19] Our results complement the present literature, showing that increasing and decreasing the concentration of small and large coils, respectively, has a small influence on adsorption. However, in OTE, polymer transport onto microspheres is significantly faster, and thus, the deviations from local-equilibrium kinetics also apply for lower molecular weight polymers. In Figure 10, we compare adsorption time series of bidisperse solutions (right panels) with corresponding monodisperse polymer (left panels) at various polymer concentrations.

When bidisperse PEO solutions bring large and small coils simultaneously to the surface, at high concentration (Figure 10a, b), the kinetics are dominated by the larger coils. Here, polymer mass transport occurs more rapidly than polymer rearrangements (~3 s), so the reduced mobility evolves similarly to the higher molecular weight monodisperse system.

When the smaller coils adsorb first, an exchange time develops for the larger chains to displace smaller ones. Here, the smaller chains initially present a barrier that becomes increasingly difficult for larger coils to penetrate. Qualitative differences are evident when comparing bidisperse and corresponding monodisperse mobility time series with $c \approx 1$ ppm PEO480K and $c \approx 6$ ppm PEO59K (Figure 10e,f). Note that, with $c \approx 2$ ppm PEO330K and $c \approx 2$ ppm PEO59K, the kinetics of the bidisperse system are similar to the higher molecular weight monodisperse polymer (Figure 10c,d).

3.5. Laser-Induced Heating and Polymer Thermodiffusion. We briefly address how laser heating affects polymer mass

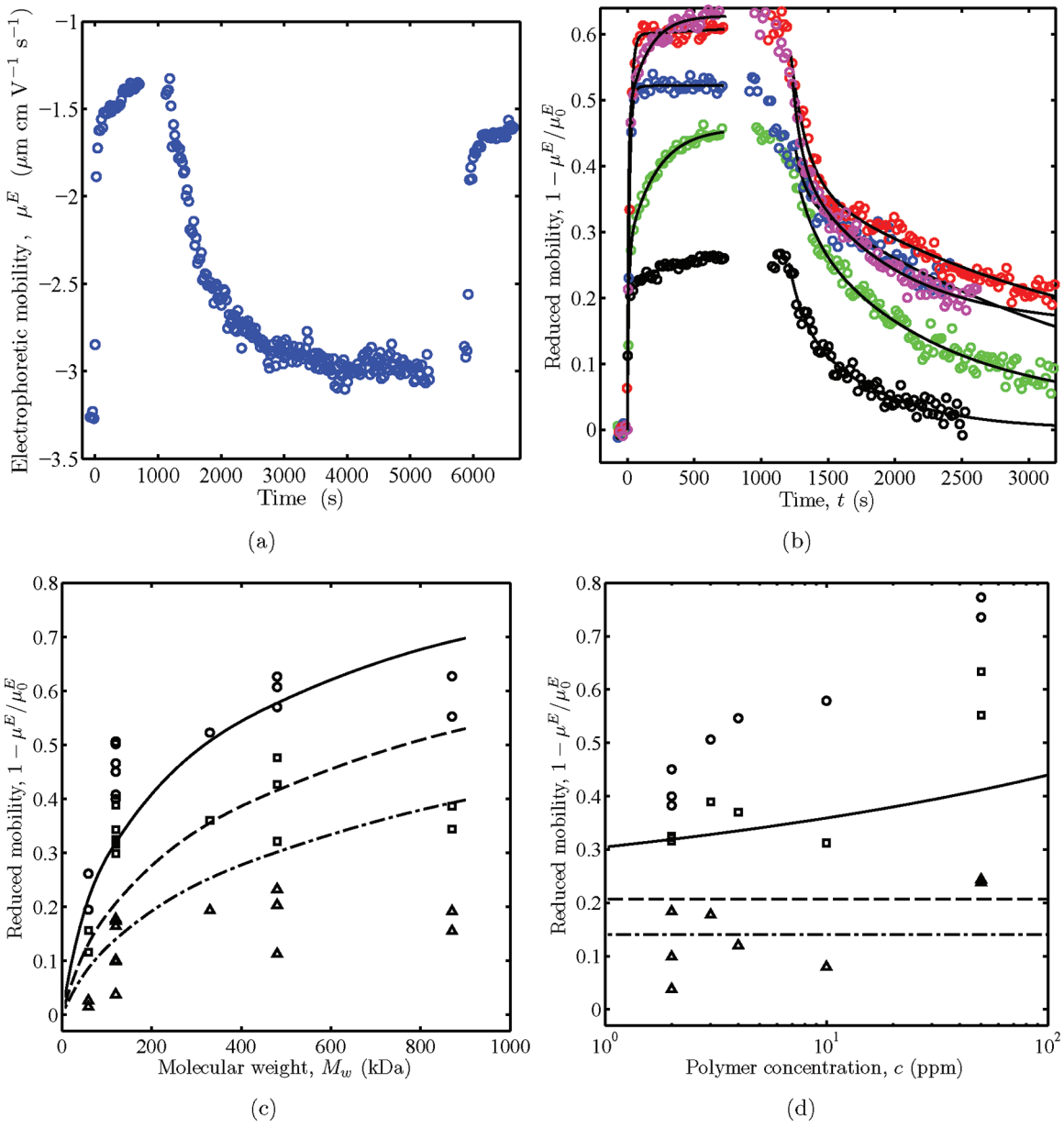

Figure 9. (a) Electrophoretic mobility μ^E time series for an initially bare silica microsphere (radius $a = 0.4\,\mu$m) exposed to polymer concentration $c \approx 4$ ppm PEO120K at $t = 0$ s (adsorption). Desorption occurs at $t \approx 1200$ s when the microsphere is abruptly re-exposed to flowing electrolyte without polymer. At $t \approx 6000$ s, the microsphere is re-exposed to the polymer solution. (b) Reduced electrophoretic mobility $\mu = 1 - \mu^E/\mu_0^E$ time series with adsorption followed by desorption of $c \approx 2$ ppm PEO59K (black), PEO330K (blue), PEO480K (red), PEO120K (green), and PEO870K (magenta). (c) Reduced mobility vs molecular weight M_w with $c \approx 2$ ppm PEO and vs c for PEO120K ($M_w = 120$ kDa) (d). Elapsed time after shutting off polymer flows: 0 s (circles), 150 s (squares), and 1500 s (triangles). Local equilibrium theory according to eq 18 for elapsed desorption times 0 s (solid), 150 s (dashed), and 1 year (dash-dotted lines). In eq 18, Sh is from eq 16 with a fluid velocity $U = 80\,\mu$m s^{-1}.

transport in OTE experiments. This is motivated by previous knowledge of optical tweezers heating samples (rates $\sim$10 K W^{-1}) at the laser focus.[25,37] We estimate diffusion-limited mass-transport rates for a heated sphere while adsorbing polymer from an aqueous solution with $Pe_D = aU/D \lesssim 1$ and $Pe_T = aU/\alpha \ll 1$, which are representative of OTE experiments. Here, D and α are the polymer molecular and thermal diffusion coefficients, respectively. Finally, we present OTE data for $c \approx 2$ ppm PEO120K adsorption at varying laser powers.

Thermodiffusion (Ludwig−Soret effect) predicts the mass transport of a molecular species along a temperature gradient ∇T.[45] Its theoretical foundation is based on molecular solvation entropy.[15] In a dilute solution, the solute molecule flux

$$\mathbf{j} = -D\nabla c - cD_T\nabla T \tag{20}$$

where c is the polymer concentration, T is the temperature, and D_T is the solute thermodiffusion coefficient. Here, we assume the microsphere behaves as an ideal sink, i.e., polymer coils that reach the surface adsorb and, therefore, $c(r = a) = 0$. After a short transient time $\gtrsim a^2/D \sim 0.1$ s, a quasi-steady polymer concentration develops around the microsphere, and the flux in eq 20 satisfies $\nabla \cdot \mathbf{j} = 0$.

dx.doi.org/10.1021/ma2003486 |*Macromolecules* 2011, 44, 8245–8260

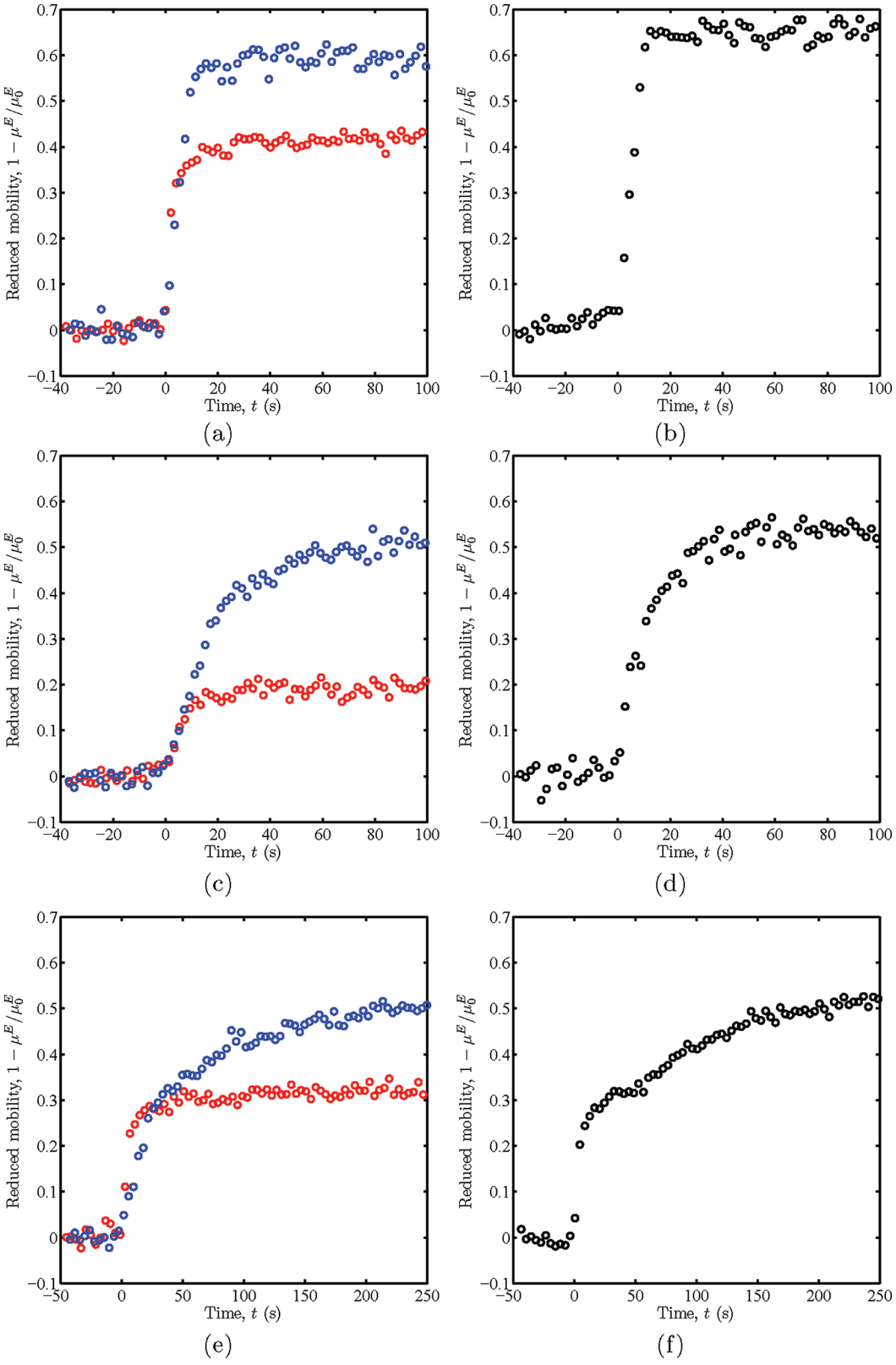

Figure 10. Reduced electrophoretic mobility $\mu = 1 - \mu^E/\mu_0^E$ time series for a bare silica microsphere (radius $a = 0.4\,\mu$m) abruptly exposed to polymer solutions at $t = 0$ s (adsorption). Time series for bidisperse polymer solutions (right panels) with concentration $c_1 + c_2$ (black) and corresponding monodisperse time series (left panels) with concentrations c_1 (blue) and c_2 (red). (a) and (b) $c_1 \approx 50$ ppm PEO330K and $c_2 \approx 50$ ppm PEO59K. (c, d) $c_1 \approx 2$ ppm PEO330K and $c_2 \approx 2$ ppm PEO59K. (e, f) $c_1 \approx 1$ ppm PEO480K and $c_2 \approx 6$ ppm PEO59K.

dx.doi.org/10.1021/ma2003486 |*Macromolecules* 2011, 44, 8245–8260

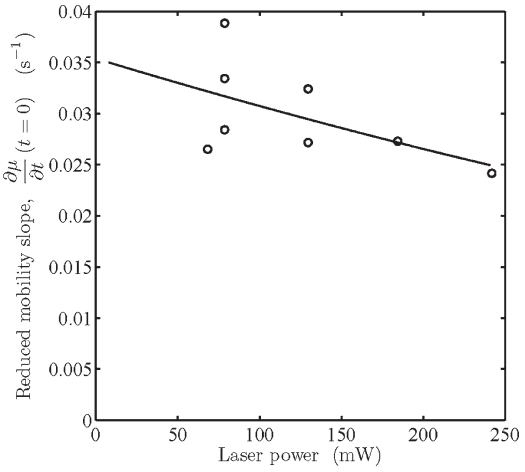

Figure 11. Reduced mobility rate of change $(\partial\mu/\partial t)(t = 0)$ vs laser power for $c \approx 2$ ppm PEO120K adsorbing onto a trapped silica microsphere with fluid velocity $U = 80$ μm s^{-1}. The line is a least-squares fit of eq 23 furnishing $S_T\Delta T = 2.75$ W^{-1}.

The temperature distribution depends linearly on laser intensity and is directly related to material absorptivities at the laser wavelength. To calculate an approximate analytical solution, we assume, for simplicity, that the sphere is heated uniformly. For microspheres, $Pe_T = aU/\alpha \lesssim 1$; thus, the quasi-steady fluid temperature satisfies $\nabla^2 T = 0$. For a sphere with radius a and surface temperature $T_0 + \Delta T$ immersed in an unbounded medium with far-field temperature T_0

$$T = T_0 + \frac{a\Delta T}{r}, \quad r \geq a \tag{21}$$

where r is the distance from the microsphere center. Substituting eq 21 into eq 20 with $\nabla \cdot \mathbf{j} = 0$ gives

$$c = c_0 \frac{e^{-S_T\Delta T a/r} - e^{-S_T\Delta T}}{1 - e^{-S_T\Delta T}} \tag{22}$$

where $S_T = D_T/D$ is the polymer Soret coefficient. Thus, the diffusion-limited polymer flux $\mathbf{j}_{\Delta T}$ onto a heated sphere increases by a factor

$$\frac{\mathbf{j}_{\Delta T}}{\mathbf{j}_0} = \frac{S_T\Delta T e^{-S_T\Delta T}}{1 - e^{-S_T\Delta T}} \tag{23}$$

where $\mathbf{j}_0$ is the flux in the absence of temperature influences. At equilibrium, the microsphere surface polymer concentration $c_s = c(a)$ is obtained by setting $\mathbf{j} = 0$ in eq 20 to obtain

$$c_s = c_0 e^{-S_T\Delta T} \tag{24}$$

Equations 23 and 24 respectively show that localized microsphere heating decreases the diffusion-limited adsorption rate and the equilibrium adsorbed amount.

Figure 11 shows how the rate of change of the mobility for $c \approx 2$ ppm PEO120K adsorption depends on laser power. The least-squares fit of eq 23 furnishes parameter estimates and errors from the Matlab functions nlinfit and nlparci, respectively. The hypothesis that the adsorption rate decreases with increasing laser power was verified with ≈90% confidence. With the exception of these experiments, all other OTE adsorption and desorption experiments in this study were performed using a laser power $P \approx 130$ mW. We find $S_T\Delta T/P \approx 2.8 \pm 2.5$ W^{-1}, where $S_T = D_T/D = 0.30$ K^{-1} with $D_T \approx 5.5 \times 10^{-12}$ m^2 s^{-1} K^{-1},[2] and D is calculated from eq 17. Thus, we estimate heating at the laser focus $\Delta T/P \approx 9.2 \pm 8.5$ K W^{-1}.

Since D_T varies little with M_w, thermodiffusion effects increase with increasing M_w. For PEO59K, PEO120K, PEO330K, PEO480K, and PEO870K, we calculate $S_T\Delta T \approx 0.24, 0.36, 0.64, 0.79$, and 1.1, and thus, with eq 23 the polymer diffusion flux decreases by factors $\mathbf{j}_{\Delta T}/\mathbf{j}_0 = 0.89, 0.83, 0.72, 0.65$, and 0.54, respectively, when $\Delta T \approx 1.2 \pm 1.1$ K for $P \approx 130$ mW.

Finally, we conclude that thermodiffusion effects due to laser heating should not be neglected in polymer adsorption experiments, especially for high molecular weight polymers. Nevertheless, the impact of thermodiffusion is not significant enough to alter conclusions drawn from our adsorption experiments, which were interpreted without accounting for thermodiffusion effects.

4. SUMMARY

We used optical tweezers electrophoresis (OTE) to measure electrophoretic mobilities of silica particles during adsorption and desorption of poly(ethylene oxide), achieving a temporal resolution of about 0.5 s. We extended the Scheutjens−Fleer equilibrium model for polymer adsorption to obtain predictions of adsorbed amount and hydrodynamic layer thickness from long-time changes in particle electrophoretic mobilities. The model describes monodisperse polymer adsorption and furnished a statistical polymer segment hydrodynamic radius $a_s \approx 39$ pm as the only fitting parameter.

Nonequilibrium polymer relaxation and reconformation dynamics affect adsorption kinetics near full coverage, especially for higher molecular weight polymers, where measured electrophoretic mobilities deviate significantly from predictions of local equilibrium theory. During adsorption, rapid transport of polymer coils to the surface is followed by polymer reconformation, lateral relaxation, and diffusion through a very thin, but dense, precursor layer. This step increases the layer thickness, which is indirectly measured by the change in particle electrophoretic mobility. Finally, for polydisperse PEO solutions, the longest adsorption time scale reflects substitution of small coils by larger ones, which are preferentially adsorbed at equilibrium.

For adsorption from monodisperse solutions, we characterized the layer growth kinetics by an apparent time to full coverage. At low polymer concentrations, this metric reflects polymer mass transport based on flow rate and polymer diffusion. However, at very high polymer concentrations, the apparent time to full coverage plateaus to a minimum value of several seconds and may be limited by polymer reconformation and lateral relaxation of the growing layer as incoming polymer attaches to the surface. For adsorption from bidisperse solutions, kinetics are dominated by the higher molecular weight coils when both (low and high molecular weight) species arrive simultaneously at high total polymer concentration. However, with low concentrations of higher molecular weight coils, the adsorption is initially dominated by small coils, which present an initial barrier that the larger chains must overcome to reach equilibrium.

Finally, desorption kinetics were faster than expected by models for local equilibrium adsorbed layers, possibly due to the high shear rates ~100 s^{-1} in our experiments. Desorbed layer thicknesses increase with the initial concentration of polydisperse polymer solutions, where a larger portion of higher molecular weight coils might have initially adsorbed.

■ ACKNOWLEDGMENT

R.J.H. gratefully acknowledges support from the Natural Sciences and Engineering Research Council of Canada and the Canada Research Chairs program; and J.A.v.H. thanks the Department of Chemical Engineering, McGill University for generous financial support through a Eugene Ulmer Lamothe graduate scholarship.

■ ADDITIONAL NOTE

[a] We solved this equation numerically using a standard finite-difference algorithm.

■ REFERENCES

(1) Adachi, Y.; Wada, T. Initial stage dynamics of bridging flocculation of polystyrene latex spheres with polyethylene oxide. *J. Colloid Interface Sci.* **2000**, *229*, 148–154.

(2) Chan, J.; Popov, J. J.; Kolisnek-Kehl, S.; Leaist, D. G. Soret coefficients for aqueous polyethylene glycol solutions and some tests of the segmental model of polymer thermal diffusion. *J. Solution Chem.* **2003**, *32*, 197–214.

(3) Churaev, N. V.; Sergeeva, I. P.; Sobolev, V. D.; Zorin, Z. M.; Gasanov, E. K. Adsorption layers of poly(ethylene oxide) on quartz studied using capillary electrokinetics. *Colloids Surf., A* **1993**, *76*, 23–32.

(4) Churaev, N. V.; Sergeeva, I. P.; Sobolev, V. D. Hydrodynamic thickness and deformation of adsorbed layers of polyethylene oxides. *J. Colloid Interface Sci.* **1995**, *169*, 300–305.

(5) Clift, R.; Grace, J. R.; Weber, M. E. *Bubbles, Drops, and Particles*; Academic Press: New York, 1978.

(6) Cohen Stuart, M. A.; Fleer, G. J. Adsorbed polymer layers in nonequilibrium situations. *Annu. Rev. Mater. Sci.* **1996**, *26*, 463–500.

(7) Cohen Stuart, M. A.; Mulder, J. W. Adsorbed polymers in aqueous media: The relation between zeta-potential, layer thickness and ionic strength. *Colloids Surf.* **1985**, *15*, 49–55.

(8) Cohen Stuart, M. A.; Waajen, F. H. W. H.; Cosgrove, T.; Vincent, B.; Crowley, T. L. Hydrodynamic thickness of adsorbed polymer layers. *Macromolecules* **1984**, *17*, 1825–1830.

(9) Couture, L.; van de Ven, T. G. M. Hydrodynamic layer thickness of poly(ethylene oxide) adsorbed on polystyrene latex. *Colloids Surf.* **1990**, *54*, 245–260.

(10) De Witt, J. A.; van de Ven, T. G. M. Kinetics and reversibility of the adsorption of poly(vinyl alcohol) onto polystyrene latex particles. *Langmuir* **1992**, *8*, 788–793.

(11) Devanand, K.; Selser, J. C. Asymptotic behavior and long-range interaction in aqueous solutions of poly(ethylene oxide). *Macromolecules* **1991**, *240* (22), 5943–5947.

(12) Dijt, J. C.; Cohen Stuart, M. A.; Hofman, J. E.; Fleer, G. J. Kinetics of polymer adsorption in stagnation point flow. *Colloids Surf.* **1990**, *51*, 141–158.

(13) Dijt, J. C.; Cohen Stuart, M. A.; Fleer, G. J. Kinetics of polymer adsorption and desorption in capillary flow. *Macromolecules* **1992**, *25*, 5416–5423.

(14) Dijt, J. C.; Cohen Stuart, M. A.; Fleer, G. J. Competitive adsorption kinetics of polymers differing in length only. *Macromolecules* **1994**, *27*, 3219–3228.

(15) Duhr, S.; Braun, D. Why molecules move along a temperature gradient. *Proc. Natl. Acad. Sci. U.S.A.* **2006**, *103* (52), 19678–19682.

(16) Fleer, G. J.; van Male, J. Analytical aproximations to the Scheutjens-Fleer theory for polymer adsorption from dilute solution. 1. Trains, loops, and tails in terms of two parameters: The proximal and distal lengths. *Macromolecules* **1999**, *320* (3), 825–844.

(17) Fleer, G. J.; Koopal, L. K.; Lyklema, J. Polymer adsorption and its effect on the stability of hydrophobic colloids. *Colloid Polym. Sci.* **1972**, *250*, 689–702.

(18) Fleer, G. J.; Cohen Stuart, M. A.; Scheutjens, J. M. H. M.; Cosgrove, T.; Vincent, B. *Polymers at Interfaces*; Chapman and Hall: London, 1988.

(19) Fu, Z.; Santore, M. M. Kinetics of competitive adsorption of peo chains with different molecular weights. *Macromolecules* **1998**, *31*, 7014–7022.

(20) Han, S.; Kim, C.; Kwon, D. Thermal/oxidative degradation and stabilization of polyethylene glycol. *Polymer* **1997**, *38*, 317–323.

(21) Hill, R. J.; Saville, D. A. 'Exact' solutions of the full electrokinetic model for soft spherical colloids: Electrophoretic mobility. *Colloids Surf., A* **2005**, *267*, 31–49.

(22) Hill, R. J.; Saville, D. A.; Russel, W. B. Electrophoresis of spherical polymer-coated colloidal particles. *J. Colloid Interface Sci.* **2003**, *258*, 56–74.

(23) Hunter, R. J. *Foundations of Colloid and Interface Science*, 2nd ed.; Oxford University Press: New York, 2001.

(24) Iler, R. *The Chemistry of Silica: Solubility, Polymerization, Colloid and Surface Properties, and Biochemistry*; Wiley: New York, 1979.

(25) Ito, S.; Sugiyama, T.; Toitani, N.; Katayama, G.; Miyasaka, H. Application of fluorescence correlation spectroscopy to the measurement of local temperature in solutions under optical trapping condition. *J. Phys. Chem. B* **2007**, *111*, 2365–2371.

(26) Källrot, N.; Linse, P. Dynamic study of single-chain adsorption and desorption. *Macromolecules* **2007**, *40*, 4669–4679.

(27) Kato, T.; Nakamura, K.; Kawaguchi, M.; Takahashi, A. Quasielastic light scattering measurements of polystyrene latices and conformation of poly(oxyethylene) adsorbed on the latices. *Polym. J.* **1981**, *13*, 1037–1043.

(28) Kawaguchi, M.; Mikura, M.; Takahashi, A. Hydrodynamic studies on adsorption of poly(ethy1ene oxide) in porous media. 2. molecular weight dependence of hydrodynamic thickness. *Macromolecules* **1984**, *17*, 2063–2065.

(29) Killmann, E.; Adolph, H. Coagulation and flocculation measurements by photon correlation spectroscopy - colloidal sio_2 bare and covered by polyethylene oxide. *Colloid Polym. Sci.* **1995**, *273*, 1071–1079.

(30) Killmann, E.; Maier, H.; Kaniut, P.; Gütling, N. Photon correlation spectrometric meaurements of the hydrodynamic layer thickness of adsorbed polyethylene oxides on precipitated silica. *Colloids Surf.* **1985**, *15*, 261–576.

(31) Lafuma, F.; Wong, K.; Cabane, B. Bridging of colloidal particles through adsorbed polymers. *J. Colloid Interface Sci.* **1990**, *143*, 9–21.

(32) Mijnlieff, P. F.; Wiegel, F. W. Intrinsic viscosity and friction coefficient of polymer molecules in solutions: Porous sphere model. *J. Polym. Sci., Polym. Phys. Ed.* **1978**, *16*, 245–263.

(33) Mubarekyan, E.; Santore, M. M. Influence of molecular weight and layer age on self-exchange kinetics for saturated layers of peo in a good solvent. *Macromolecules* **2001**, *34*, 4978–4986.

(34) Ohshima, H. Electrophoretic mobility of soft particles. *J. Colloid Interface Sci.* **1994**, *163*, 474–483.

(35) Pattanayek, S. K.; Juvekar, V. Prediction of adsorption of nonionic polymers from aqueous solutions. *Macromolecules* **2002**, *35*, 9574–9585.

(36) Pelssers, E. G. M.; Cohen Stuart, M. A.; Fleer, G. J. Kinetics of bridging flocculation. role of relaxations in the polymer layer. *J. Chem. Soc., Faraday Trans.* **1990**, *86*, 1355–1361.

(37) Peterman, J. G.; Gittes, F.; Schmidt, C. F. Laser-induced heating in optical traps. *Biophys. J.* **2003**, *84*, 1308–1316.

(38) Scheutjens, J. M. H. M.; Fleer, G. J. Statistical theory of the adsorption of interactinig chain molecules. 1. partition function, density ditribution, and adsorption isotherms. *J. Phys. Chem.* **1979**, *83*, 1619–1635.

(39) Scheutjens, J. M. H. M.; Fleer, G. J. Statistical theory of the adsorption of interactinig chain molecules. 2. train, loop and tail size distribution. *J. Phys. Chem.* **1980**, *84*, 178–190.

(40) Trens, P.; Denoyel, R. Conformation of poly(ethy1ene glycol) polymers at the silica/water interface: A microcalorimetric study. *Langmuir* **1993**, *9*, 519–522.

(41) van de Ven, T. G. M. *Colloidal Hydrodynamics*; Academic Press: New York, 1989.

(42) Van der Beek, G. P.; Cohen Stuart, M. A.; Cosgrove, T. Polymer adsorption and desorption studies via lh nmr relaxation of the solvent. *Langmuir* **1991**, *7*, 327–334.

(43) van Heiningen, J. A.; Hill, R. J. Polymer adsorption onto a micro-sphere from optical tweezers electrophoresis. *Lab Chip* **2010**, *11*, 152–162.

(44) van Heiningen, J. A.; Mohammadi, A.; Hill, R. J. Dynamic electrical response of colloidal micro-spheres in compliant micro-channels from optical tweezers velocimetry. *Lab Chip* **2010**, *10*, 1907–1921.

(45) Wiegand, S. Thermal diffusion in liquid mixtures and polymer solutions. *Am. J. Phys.: Condens. Matter* **2004**, *16*, R357–R379.

(46) Wind, B.; Killmann, E. Adsorption of polyethylene oxide on surface modified silica — stability of bare and covered particles in suspension. *Colloid Polym. Sci.* **1998**, *276*, 903–912.